Effect of Mass Injection on the Drag of a Slender Cone in Hypersonic Flow

HARTLEY H KING* AND LAWRENCE TALBOT†
University of California, Berkeley, Calif

The influence of air and helium injection on the drag force and of pressure distribution on a porous 5° half-angle cone was investigated at Mach numbers of 3 9 and 5 6, with freestream Reynolds numbers of 1800 and 6200/in , respectively It was found that gas injection into the cone boundary layer increased the self-induced surface pressure markedly, but reduced the total drag of the cone slant surface by as much as 50% A surprising result of the experiment was that air injection was nearly twice as effective as the same mass flow of helium injection in reducing the total drag It is possible that this contradiction to simple boundary-layer theory may be due to transverse curvature and self-induced pressure gradient effects An approximate analysis of the flow, including viscous interaction and transverse curvature effects, agreed reasonably well with the data for zero mass injection, but the agreement became progressively poorer with increased mass injection

Nomenclature

A = area
C = Chapman-Rubesin factor
C_D = drag coefficient
C_f = skin-friction coefficient
D = drag force
f_w = nondimensional injection rate parameter [Eq (6)]
M = Mach number
$\dot{M}$ = total mass injection rate
P = pressure
R = gas constant
Re = Reynolds number
r_w = local cone radius
T = temperature
u = velocity, x direction velocity in the boundary layer
v = y direction velocity in the boundary layer
x = distance along cone ray from apex
y = distance normal to cone surface
Z = axial distance along the cone
α = cone half-angle
δ^* = displacement thickness
μ = viscosity
ρ = density

Subscripts

b = base
c = inviscid conical flow value
f = due to skin friction
g = gross
inj = due to injection
M = without viscous interaction or transverse curvature
p = due to pressure
s = stagnation
w = at the wall
δ = at the outer edge of the boundary layer
∞ = undisturbed freestream conditions

1 Introduction

AERODYNAMIC behavior in the hypersonic low-density regime is governed by a complicated interaction between the boundary layer and the outer flow over the body [1-4] Mass transfer (arising either from ablation or controlled gas injection) can increase greatly the displacement thickness of the boundary layer,[5 6] and thus affect profoundly this entire viscous interaction phenomenon An interesting and important aspect of mass transfer, therefore, is its effect on the aerodynamic behavior of a slender body in hypersonic low Reynolds number flow, where viscous interaction effects are important even in the absence of mass transfer

The main object of the present study was the experimental investigation of the effect of gas injection on the drag and pressure distribution on a 5° half-angle porous cone Both helium and air injection were employed at two Mach-Reynolds number combinations in the Berkeley low-density wind tunnel This report presents a general discussion of the experiment, the experimental data obtained, and the comparison of these data with theory Additional details of the experiment can be found in Ref 7

2 Experimental Program

The experiments were conducted in the low-density wind tunnel of the University of California Rarefied Gas Dynamics Laboratory This wind tunnel is a free-jet, continuous flow facility which expands room-temperature air through an axisymmetric nozzle to a test chamber pressure of about 85 μ of mercury The flow characteristics and calibrations of the two nozzles used in the present experiment have been described in previous reports [8 9] Additional data and an analysis of experimental accuracy of the determination of the flow characteristics are presented in Ref 7

The properties of the two flow conditions employed in the experiments are given in Table 1

2 1 Models

All models used in the experiment were 5° cones of 3 5-in length and are shown schematically in Fig 1 The porous models were of uniform wall thickness and, because of fabrication requirements, had small solid tip and base regions Each of the porous-wall pressure models (called the 1,3,5 and 2,4,6 models) had three in-line taps made by attaching 0 040 × 0 007-in wall stainless-steel tubing to the surface with epoxy resin A third model without taps (called the force model) was used for the drag force measurements The porous models were fabricated commercially from sintered powdered Monel metal particles of less than 0 0005-in diam The injection gas was introduced into the porous models through a hollow tail sting located inside a conical

Received April 26, 1963; revision received March 2, 1964 This work was jointly supported by the General Electric Company under Purchase Order 214-J91534 and the Office of Naval Research under Contract N-onr-222(45)

* Formerly Graduate Student in Aeronautical Sciences; presently at Electro-Optical Systems, Pasadena, Calif Member AIAA

† Professor of Aeronautical Sciences Member AIAA

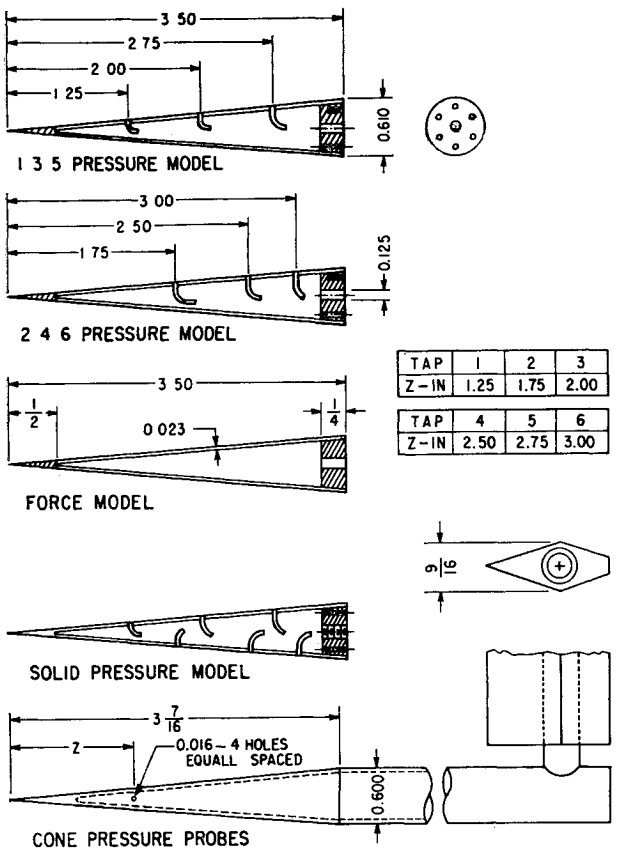

Fig 1 Model dimensions

afterbody, as shown in Fig 2 This afterbody configuration was adopted mainly to simplify the analysis of the various drag force contributions

The small size of the porous models caused some difficulty in the attachment of the pressure taps Although the taps were locally smooth to the touch, localized wrinkling of the thin (0 023 in) porous wall around the taps was found, which apparently resulted in systematic errors in the pressures measured on the porous models In addition, the wall inclination deviated slightly (but symmetrically) from the specified 5° angle where the solid tip was joined to the porous wall Further back, the surface angle was determined to be 5 ± 0 03°

A solid brass model of better surface and tap quality was constructed to investigate the magnitude of the errors caused by the imperfections on the porous models This is called the "solid pressure model" It was geometrically similar to the porous pressure models and had the same pressure tap construction ‡

An additional series of solid brass models (called the "cone probes") were also used to measure the zero-injection pressure distribution and to determine if a pressure orifice size effect existed Each of these models had four 0 016-in taps located at 90° intervals around the circumference at a location corresponding to one of the porous model pressure taps

All models except the cone pressure probes were mounted in the afterbody configuration shown in Fig 2 The cone probes were attached directly to the tunnel rotating probe mount

Table 1 Experimental flow conditions

M_∞	$(\rho_\infty u_\infty^2)/2$, torr	$(Re/\text{in})_\infty$, in $^{-1}$	P_∞, torr	T, °F	P/P_∞
3 93	0 914	1765	0 0848	540	1 272
5 64	1 895	6200	0 0852	539	1 494

‡ On the solid model the 1,3,5 and 2,4,6 taps were in line on cone rays 180° apart

2 2 Injection Gas Flow

The injection gas flow system is shown schematically in Fig 3 Metering was accomplished both by a Fischer-Porter "flowrator" meter and by measuring pressure drops across glass capillaries All of the metering equipment was calibrated over the full range of experimental injection rates using both air and helium The uncertainty in M is estimated to be about ±3%

A crude (± 20% possible error) measurement of the injection distribution for the three porous models was made, and the results are shown in Fig 4 The local flux was determined by masking off various axial lengths Z of the porous cones with rubber tubing and obtaining flow rate vs covered length for constant pressure drop across the model at atmospheric pressure The local flux was then calculated from the derivative dM/dZ of these data The local variations in mass flux can be attributed in part to the blocking effect of the pressure tubulation within the models

2 3 Pressure Measurements

To obtain short response times, all model pressures were measured with a Decker transducer located close to the models within the wind tunnel The transducer was calibrated against a precision oil manometer,[10 11] as indicated in Fig 3 Pressures measured on the 1,3,5 and 2,4,6 porous injection models exhibited considerable scatter because of the surface imperfections mentioned earlier and because of hole size effects [2] The latter effects were manifested also in the surface pressures on the "solid pressure model," which, however, gave much more consistent readings than the porous models The cone probe models gave the most consistent results, which agreed well with previous data [1 2] The cone probe models were therefore adopted as the standard for the no-injection surface pressures, and the pressures measured on the porous injection models were corrected by normalizing them with respect to the cone probe pressures

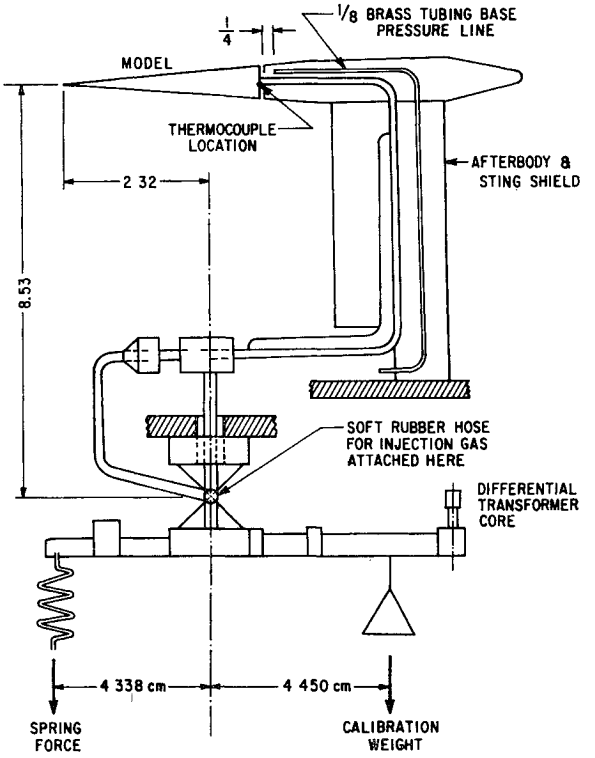

Fig 2 Mounting of the force model

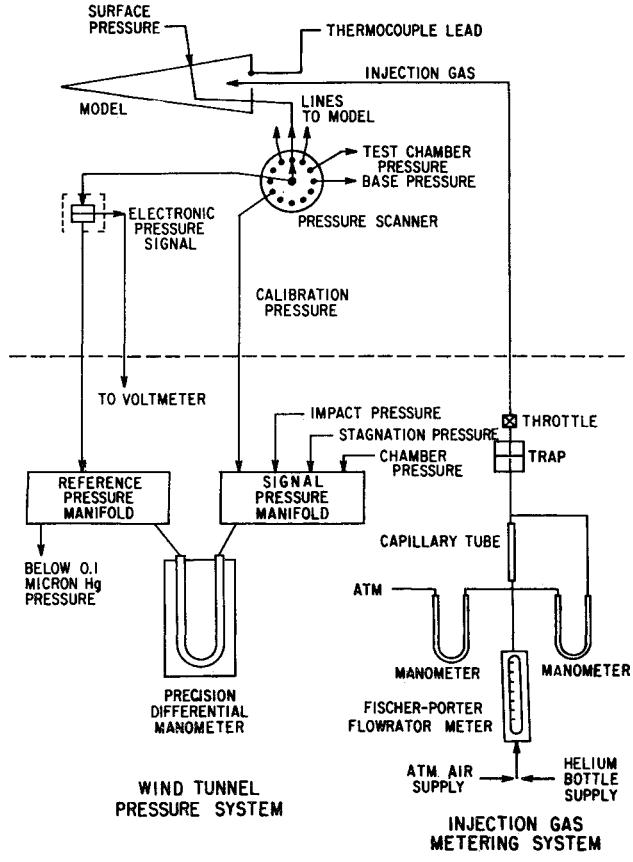

Fig 3 Injection flow and pressure system

This normalization consisted of the following correction:

$$P_c = P_{m\,as}\left(\frac{P_{\text{cone pr}}}{P_{\bar{M}=0}}\right) \qquad (1)$$

The correction for almost all data points amounted to less than 15%

As was expected, mass injection increased the induced pressure Helium injection produced a greater pressure increase than did air injection, and for the same gas the pressure increase was greater at the higher Mach number The data are plotted in Figs 5 and 6 in the form of the (corrected) induced pressure increment $(P - P)/P$ where P_c is the inviscid cone surface pressure[12 13] given in Table 1 The data points are identified by values of the injection parameter f_w, which is related to the total injection mass flux M through formulas derived in the Appendix and plotted in Fig 7, as explained later The theoretical curves plotted in Figs 5 and 6 likewise will be discussed subsequently

The base pressure was found to be increased somewhat by helium injection, but remained practically constant in the case of air injection Detailed data are presented in Ref 7,

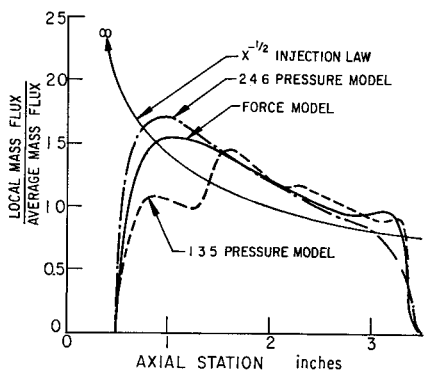

Fig 4 Local mass flux distribution

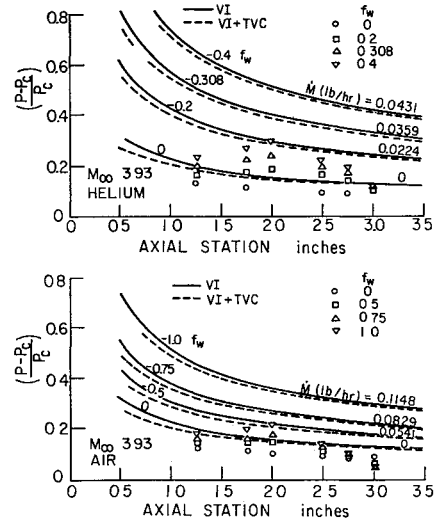

Fig 5 Comparison of measured self-induced pressures with values predicted by the present theory

and only the average base drag $P_b A_b$ will be presented here in the drag analysis Over the range of experimental conditions, the base pressure ranged from about 0 9 P to 1 2 P_c Undoubtedly some variation in pressure over the base existed, but this variation can be neglected as a second-order effect, since, as will be seen, the total contribution of the base drag was itself small

2 4 Drag Force Measurements

A third porous model without pressure taps (the force model) was used for the gross drag measurements The one-component flexure-pivot force balance used in these tests is shown schematically in Fig 2 The balance beam torque due to model force is counteracted by a spring whose extension may be changed to "null" the position of the beam, the null position being sensed electrically The spring extension is controlled by a micrometer screw and may be determined to the nearest 0 001 in [4]

The force-measuring procedure used was to obtain first a "wind off," or tare spring extension reading without injection The flow was then turned on and a "wind on" reading was taken, with or without injection The difference between these two readings thus measured the "gross" aerodynamic force on the model The "total" drag is defined as the drag

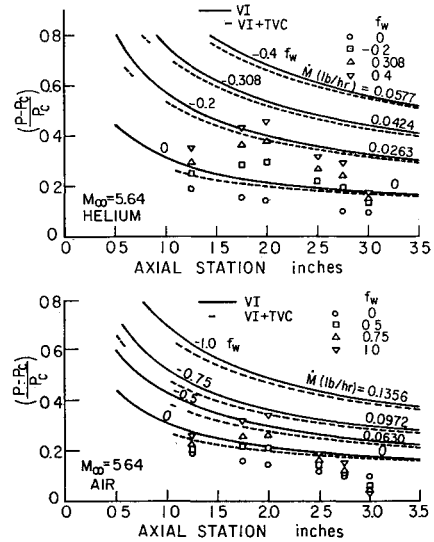

Fig 6 Comparison of measured self-induced pressures with values predicted by the present theory

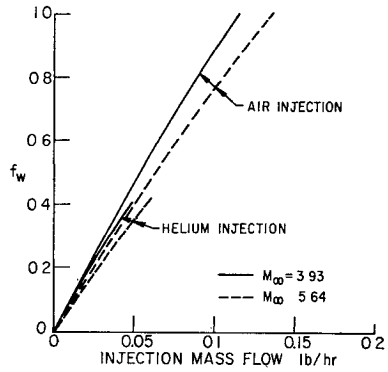

Fig 7 Relation between injection parameter f_w and the total injection rate (from present theory)

due to all forces on the cone slant face and was obtained by subtracting the drag due to base pressure from the measured "gross" drag The base drag was assumed equal to the base pressure times the total base area

The measured gross drag of the model is the algebraic sum of the drag due to skin friction, slant surface pressure, base pressure, and momentum flux of the injected gas For a theoretical comparison, it is of interest to compute each of these separate contributions All drag contributions are given in terms of drag coefficients referred to the cone base area, namely,

$$C_D = D/(\rho_\infty u_\infty^2/2)A_b \quad (2)$$

Gross drag data are shown in Fig 8 It may be observed that these data are quite "smooth," with relatively little scatter

The relation between the various drag coefficients is as follows:

$$C_{D_{tot}} = C_{D_g} - C_{D_b} \quad (3)$$

$$C_{D_{tot}} = C_{D_f} + C_{D_p} + C_{D_{inj}} \quad (4)$$

Equation (3) defines the experimental "total" drag, and the pressure drag was obtained by integration of the (smoothed) experimental pressure distribution data of Figs 5 and 6 $C_{D_{inj}}$ was a small contribution that was evaluated theoretically (see Appendix) and C_{D_f} was then determined from Eq (4)

In order to treat the drag results in a convenient manner, curves were faired through the gross drag and base pressure data The various drag contributions were then computed from the faired curves at evenly spaced values of the injection rate For this reason, actual data points do not appear in most of the subsequent figures

Figure 9 shows the experimental "total" drag results, which were obtained by correcting the data of Fig 8 for the effects of base pressure (The magnitude of this correction was about 10%) One sees, as expected, that the injection caused a significant decrease in total drag over the range of injection rates of the experiment The most interesting feature of these data, however, is that the air injection was more efficient in reducing the total drag than was helium This contradicts simple boundary-layer theory, which predicts that the helium curve should lie below the air injection curve [14] The bars on the curves of Fig 9 indicate the possible uncertainty due to experimental and data reduction errors, as discussed in Ref 7

The relative magnitudes of the various experimental drag contributions are shown in Figs 10 and 11 Here it may be seen that skin friction contributes the largest portion of the total drag (about 70—85%) The injection drag is relatively insignificant, although helium injection contributes a greater amount than air at the same mass injection rate because of higher efflux velocity The pressure drag is small at zero injection (less than about 15% of the total drag),

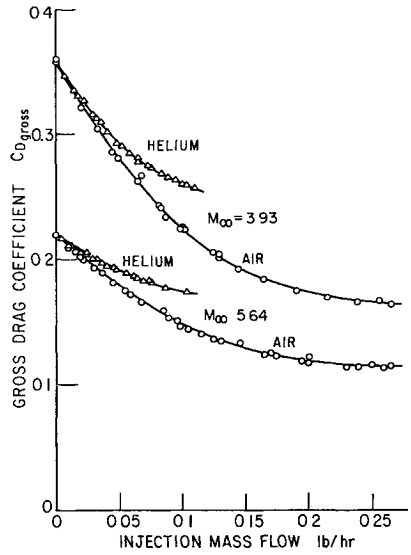

Fig 8 Gross drag coefficient experimental data

but becomes more important with increasing injection (more so with helium than with air) This is primarily the reason for the larger separation between the air and helium total drag curves of Fig 9 than between corresponding skin-friction curves of Figs 10 and 11 However, since in Figs 10 and 11 the skin-friction curves for helium injection are still higher than those for air, the pressure-plus-injection drag alone could not account for the greater total drag with helium injection shown in Fig 9

2 5 Surface Temperature

The model temperature, as measured by a single thermocouple located at the model base, increased slightly with injection These temperatures were not recovery temperatures, since the model was not thermally isolated However, the indication was that of increasing recovery factor with injection, in qualitative agreement with the predictions of Freedman et al [18]

3 Comparison with Theory

3 1 Surface Pressures

Figures 5 and 6 show the comparison between the measured surface pressures and those computed from the viscous inter-

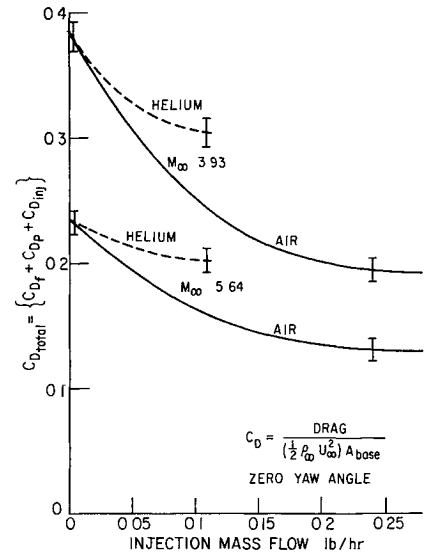

Fig 9 Faired experimental total drag data

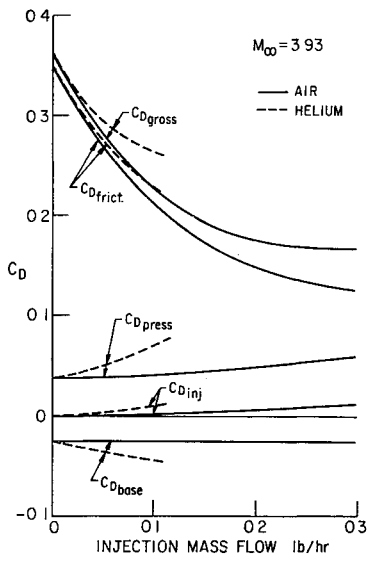

Fig 10 Drag contributions based on experimental data

action theory described in the Appendix One sees from these graphs that the viscous interaction theory overestimates the induced pressure by at least a factor of 2 The transverse curvature correction to the induced pressure is in the right direction, but it is too small to account for the discrepancy

It is perhaps not surprising that the theory and experiment disagree First, the theory assumes that the mass injection $\rho_w v_w$ varies as $x^{-1/2}$ § The actual measured injection variation is shown in Fig 4, together with the curve representing the $x^{-1/2}$ law for the same $\dot{M}$ With an $x^{-1/2}$ law, the injection increases indefinitely as the cone apex is approached, and this accounts for the high self-induced pressure increment $(P - P)/P_c$ predicted by the theory near the nose The drop-off in experimental pressure near the rear of the cone is probably due to the upstream influence of the solid afterbody and the gap at $Z = 3\,5$ in , and this is not accounted for in the theory

Other possible sources for the discrepancies between the experimental and theoretical pressure distributions are the use of tangent cone theory for the inviscid flow (which, in general, overestimates the induced pressure[1,2]), the assumption of local similarity, and the neglect of the pressure gradient terms in the boundary-layer theory The use of the no-injection transverse curvature theory for TVC (transverse curvature) corrections with injection probably results in an overestimate, since one might expect the thicker boundary layers produced by injection to be proportionally more subject to TVC effects It would be of some interest to obtain more precise data on pressure variation with mass injection using better models, since the discrepancy between theory and experiment is somewhat larger than might have been anticipated from previous comparisons between theory and experiment without mass injection

3 2 Total Drag

Figures 12 and 13 show a comparison of the faired experimental total drag data with the results of the present theory for the two experimental flow conditions The curves labeled no VI (viscous interaction) or TVC are based on the analyses of Baron[5] and Low[6] for skin-friction drag, but they use the inviscid flow quantities for boundary-layer edge values and pressure drag Thus, these curves give the estimated drag based on simple boundary-layer theory (with an $x^{-1/2}$ injection law) The curves labeled VI are the results of the calculations including the viscous interaction effect Finally, the curves labeled VI + TVC include a transverse curvature correction

It may be seen from Figs 12 and 13 that the inclusion of the VI and TVC effects produce a considerable improvement over the usual high Reynolds number boundary-layer theory. In fact, for zero injection, the experimental and VI + TVC values for total drag are within 5% for both flow conditions This good agreement is probably fortuitous, considering the empirical nature of the theory For example, no-injection weak interaction theory predicts that the local skin-friction coefficient C_f should increase slightly over the no-interaction value C_{fM} because of the influence of the self-induced favorable pressure gradient [3] Maslach and Talbot[4] have estimated that the magnitude of this effect is approximately

$$C_{f\mathrm{VI}}/C_{fM} \approx (P/P)_{\mathrm{VI}}^{1/2} \tag{5}$$

The method of analysis used here, which neglects the pressure gradient, actually predicts a slight decrease in the local skin friction due to viscous interaction effects This decrease comes about from the variation in boundary-layer edge properties due to matching of the boundary layer to the external flow and the use of skin-friction coefficients based on the flat-plate boundary-layer theory for the local edge condition (the local similarity hypothesis) The error made in neglecting the increase in skin-friction drag due to pressure gradient is at least partly cancelled by the error made in neglecting the effect of the pressure gradient in thinning the boundary layer and reducing the viscous interaction pressure drag increment

One sees from Figs 12 and 13 that the agreement between experiment and theory becomes rapidly worse with increasing injection One possible cause for the discrepancy has already been mentioned, namely, the use of a TVC correction applicable only to the zero-injection case Another possible source of the discrepancy is the effect of pressure gradient on the boundary layer, in this case the self-induced pressure gradient due to viscous interaction effect Baron and Scott[17] have considered the influence of a favorable pressure gradient on a flat-plate boundary layer with both helium and air injection Their numerical results were obtained only for the limiting case of $M_\infty \to 0$, and they are not really applicable to the present experiments Interestingly, Baron and Scott found that the local skin friction could be nearly doubled by favorable pressure gradients of the order of the maximum gradients found in the present experiments,

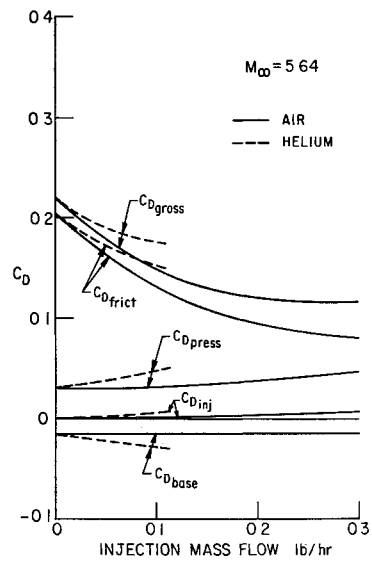

Fig 11 Drag contributions based on experimental data

§ This is not exactly true, since in Eq (A7) the quantity $\rho_\delta u_\delta \mu_\delta C$ varies with x because of viscous interaction

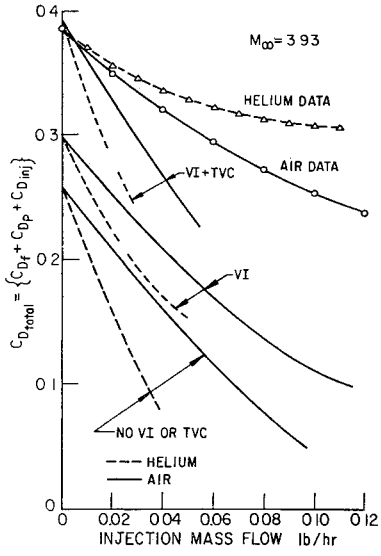

Fig 12 Effect of viscous interaction and transverse curvature on total drag according to the present theory, and compared with experimental data

both with and without mass injection Even more interesting, however, is the fact that their results show that, while at zero pressure gradient, the reduction in skin friction is greater for helium injection than for air injection; this trend is reversed for moderate, favorable pressure gradients, and air injection becomes more effective than helium in reducing the skin friction

An attempt was made to determine whether this last result of Baron and Scott could account for the anomalous higher drag obtained with helium injection The method consisted of computing the local changes in the skin-friction coefficient due to pressure gradient, taking for the pressure gradient that which was obtained from viscous interaction calculations Mach number terms that Baron and Scott annulled in their pressure gradient parameter were kept (these Mach number terms increase the effective pressure gradient), although the differential equations themselves still apply only for the case $M \to 0$ The net effect was to increase both the helium and air injection drag curves of Figs 12 and 13 (those labeled VI + TVC) by roughly 10% No appreciable change in the relative effectiveness of drag reduction by helium and air injection from that obtained in the VI + TVC calculations was found, however ¶ These pressure gradient estimates have not been presented because the appropriateness of applying the Baron and Scott incompressible results to the present problem cannot be assessed without extensive additional calculations Correspondingly, the fact that these estimates did not resolve the anomalous drag behavior does not preclude the possibility that a pressure gradient analysis, which takes proper account of compressibility, might provide a satisfactory explanation for the data The recent work of Smith and Clutter,[20] which became available to the authors after the present study was completed, merits investigation

4 Conclusions

For the two flow conditions of the tests, both helium and air injection produced significant reductions in the total drag of the 5° cone The seemingly anomalous feature of the drag data was, however, that the incremental drag reduction with air injection was up to about twice that with helium The zero-injection drag results agreed reasonably with an approximate boundary-layer theory With increasing injection rates the theory became progressively worse, possibly because of the neglect of pressure gradient effects and because an adequate transverse curvature correction was unavailable

The experiments showed that both helium and air injection increased the boundary-layer-induced surface pressure increment up to five times the no-injection value at a given station on the cone The theory agreed with the trend of the data with injection, but it overestimated the induced pressure increment by a factor of about two

The experimental fact that helium injection was less effective than air for total drag reduction suggests the possibility that injected or ablated materials of high molecular weight may be more effective than light gases for reducing the drag of slender bodies in the low Reynolds number flight regime This conclusion must remain tentative, however, until the combined effects of viscous interaction, transverse curvature, and pressure gradient have been properly assessed It would be desirable to carry out a similar experimental study on a two-dimensional shape, such as a slender wedge, to determine if the anomalous drag reduction is entirely a three-dimensional effect If the anomaly is caused by induced pressure gradients, it should appear in even more pronounced fashion on a slender wedge, since the induced pressure gradients in two-dimensional flow are stronger than in axisymmetric flow

Appendix: Theoretical Analysis

A truly realistic description of the boundary-layer flow for the experiment is beyond the scope of the present report The present analysis is an "engineering approach" that attempts to explain the major trends in the data, but which is simple enough to be done by hand calculations with a reasonable expenditure of effort The analysis makes liberal use of existing boundary-layer solutions for a flat plate with surface mass flux varying as $x^{-1/2}$, as required by similarity considerations [5,6]

It is clear that the problem can be made tractable only by the omission from the analysis of most of the complicating boundary-layer effects Talbot, Koga, and Sherman[1] have shown that induced surface pressure distribution may be estimated with reasonable accuracy for the no-injection case by considering only the viscous interaction coupled to a locally similar boundary layer Their analysis assumed that viscosity was proportional to temperature and that compressibility effects could be accounted for by the Chapman-Rubesin factor These assumptions are retained in the present

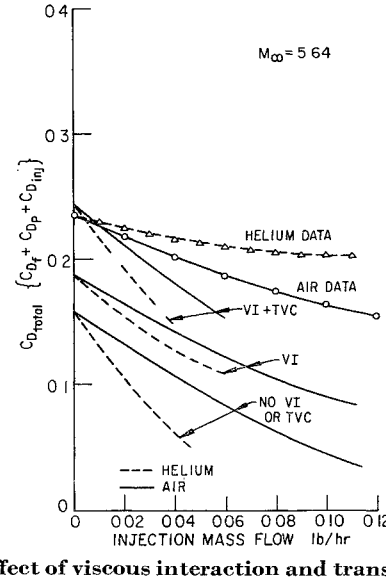

Fig 13 Effect of viscous interaction and transverse curvature on total drag according to the present theory, and compared with experimental data

¶ This conclusion is unaltered if the experimental pressure gradient is used instead of the theoretical one in the calculation

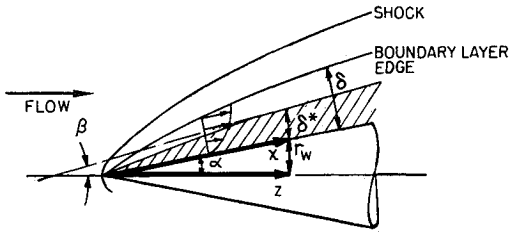

Fig 14 Assumed physical model of the flow

analysis, with viscosity being assumed proportional to temperature times a function of mass concentration for the air-helium mixture [5] In the latter case, Baron[5] has shown that the problem may be formulated so that the Chapman-Rubesin factor is chosen for air only, in the same manner as for the single component boundary layer In the present analysis, the method of Talbot, Koga, and Sherman is extended to include the effects of surface mass transfer on the induced pressure and also on the total skin-friction drag

Inviscid Flow

In order to solve the boundary-layer problem one must know the outer-edge boundary conditions from the inviscid flow solution Since these conditions depend on the boundary-layer growth, the inviscid and boundary-layer flows must be considered together Following Talbot,[1 2] the displacement thickness δ^* is added to the cone at each station x as shown in Fig 14 Boundary-layer edge quantities ρ_δ, u_δ, etc , are then assumed to be given by the tangent cone theory[3] applied to the effective body formed by the addition of δ^* to the cone Using this procedure, the specification of the boundary-layer edge conditions can be made once M_∞ and the local tangent cone angle β given by

$$\beta = \alpha + \arctan (d\delta^*/dx) \tag{A1}$$

are known

Displacement Thickness

The effect of transverse curvature on the displacement thickness[15 16] is neglected and the results of Low[6] for air injection and Baron[5] for helium injection are employed In both cases the expression for the displacement thickness may be written, using the Mangler transformation

$$\delta^* = 2(\mu_\delta Cx/3\rho_\delta u_\delta)^{1/2}[\zeta + (\gamma - 1)M_\delta^2 I_r/2 + I\,(T_w - T_{aw})/T_\delta] \tag{A2}$$

where ζ, I , and I are constants for a given mass injection rate (assuming a locally similar boundary layer) The adiabatic wall temperature in Eq (A2) is specified in terms of the recovery factor σ as follows:

$$T_{aw}/T_\delta = 1 + \sigma(\gamma - 1)M_\delta^2/2 \tag{A3}$$

and the Chapman-Rubesin factor C for both injection gases is determined by matching the air viscosity at the wall:

$$C = (\mu_w T_\delta)/(\mu_\delta T_w) \qquad \mu = \mu_{\text{air}} \tag{A4}$$

An approximate value of $d\delta^*/dx$ is obtained by neglecting the streamwise derivatives of boundary-layer edge quantities, so that

$$d\delta^*/dx = (\mu_\delta C/3\rho_\delta u_\delta x)^{1/2}[\zeta + (\gamma - 1)I\,M_\delta^2/2 + I\,(T_w - T_{aw})/T_\delta] \tag{A5}$$

This approximation is in the spirit of the local similarity assumption of the boundary-layer analysis When M_∞ and the tangent cone angle β are specified, one may find the edge Mach number M_δ and pressure P_δ by interpolation in the conical flow tables of Sims [13] The remaining edge quantities are determined from the formulas

$$\begin{aligned} T/T_\infty &= [1 + (\gamma - 1)M_\infty^2/2] \\ \rho_\delta/\rho_\infty &= (P_\delta T_\infty)/(P_\infty T_\delta) \\ T_s/T_\delta &= [1 + (\gamma - 1)M_\delta^2/2] \\ u_\delta &= (\gamma R_i T_\delta)^{1/2} M_\delta \end{aligned} \tag{A6}$$

and the viscosity $\mu = \mu_\delta(T_\delta)$ was determined from the Bromley-Wilke viscosity data [19]

The quantities ζ, I_r, and I_s in Eq (A5) depend on the dimensionless mass injection parameter f_w and are given in Table 2

Injection Mass Flow Rate

According to the analyses of Baron[5] and Low,[6] the local mass flux is given by

$$\dot{m} = \rho_w v_w = -(\tfrac{1}{2})f_w(3\rho_\delta u_\delta \mu_\delta C/x)^{1/2} \tag{A7}$$

The total mass flow rate $\dot{M}$ is determined by integration,

$$\dot{M} = \int_{A_{\text{slant}}} \rho_w v_w dA = -\pi \sin\alpha \int_0^l (3\rho_\delta u_\delta \mu_\delta C x)^{1/2} f_w dx \tag{A8}$$

Since the quantities I_r, I , and ζ have been computed for only a few values of f_w, and the edge quantities $\rho_\delta u_\delta \mu_\delta C$ in Eq (A7) are initially unknown, it is impractical for the present purposes to specify the local flux $\rho_w v_w$ in advance Instead, f_w (const) is taken as the independent mass flux parameter, and the total mass injection rate $\dot{M}$ corresponding to f_w can be determined from Eq (A8) once $\rho_w v_w$ is known Because of the variation of the edge quantities ρ_δ, u_δ, etc with x caused by viscous interaction, the injection law will no longer be the $x^{-1/2}$ variation given by (A7) for constant edge quantities In fact, one loses control of the injection law altogether by this procedure and must accept whatever distribution comes out of the assumption that f_w is constant Calculations showed, however, that viscous interaction did not change the injection distribution more than about $\pm 10\%$ from the $x^{-1/2}$ law

Solution Method

The matching of the boundary layer and inviscid solutions at each station x is conveniently done by graphical analysis in a manner similar to that employed in Ref 1 This matching yields the proper displacement thickness slope angle β for the value of x under consideration With β known, the boundary-layer edge quantities can be calculated from the tangent-cone tables and Eqs (A6) By assuming a locally similar boundary layer, then, the results of Baron[5] and Low[6] become available for the computation of skin friction and total mass injection rate Since the pressure is approximately constant across the boundary layer, the surface pressure distribution is the same as P_δ

Table 2 Values appearing in the expressions for displacement thickness and skin friction

Air injection (after Low[8])					
f_w	σ	ζ	I	I_s	f_w''
0	0 848	0 860	1 109	0 969	1 328
−0 50	0 799	1 230	1 411	1 317	0 658
−0 75	0 768	1 564	1 660	1 623	0 374
−1 00	0 733	2 195	2 103	2 202	0 142
Helium injection (after Baron[5])					
f_w	σ	ζ	I_r	I_s	Kwf_w''
0	0 848	0 860	1 109	0 969	1 328
−0 20	0 745	1 933	1 704	1 961	0 767
−0 308	0 674	2 671	2 027	2 650	0 503
−0 40	0 616	3 510	2 345	3 393	0 307

The remaining quantities of interest are the skin-friction drag and pressure drag coefficients From Baron and Low the local skin-friction coefficient is given by

$$C_f = (\tfrac{1}{2})[(3\mu_\delta C)/(\rho_\delta u_\delta x)]^{1/2} K_w f_w'' \quad \text{(A9)}$$

Values of $K_w f_w''$ are given in Table 2 $K_w = 1\,0$ for air injection The skin-friction drag is then obtained by integration,

$$C_{D_f} = \left(\frac{K_w f_w''}{\rho_\infty u_\infty^2 l^2 \tan\alpha}\right) \int_0^l \left(\frac{3\mu_\delta C x}{\rho_\delta u_\delta}\right)^{1/2} \rho_\delta u_\delta^2 dx \quad \text{(A10)}$$

The pressure drag coefficient is obtained from an integral of the surface pressure distribution as follows:

$$C_{D_p} = \left(\frac{4}{\gamma M_\infty^2 l^2}\right) \int_0^l \left(\frac{P_\delta}{P_\infty} - 1\right) x\, dx \quad \text{(A11)}$$

The results of the foregoing analysis are shown by curves labeled VI (for viscous interaction solution) in the figures

Transverse Curvature Effect

No analysis of the boundary-layer equations with both foreign gas injection and transverse curvature terms has been carried out to the authors' knowledge For the zero-injection case, however, Yasuhara[16] has solved approximately the TVC boundary-layer equations for the case of zero pressure gradient, Prandtl number equal to 0 7, and $T_w/T_s = 1\,0$ This is sufficiently close to the present experimental conditions to warrant a quantitative estimate of the TVC effect based on his calculations It will be assumed that Yasuhara's results may be applied also for the injection case, although there is, of course, no reason to expect that zero-injection TVC corrections will provide good approximations for the injection case

The boundary-layer-induced pressure depends on the displacement thickness slope $d\delta^*/dx$ One may use Yasuhara's results to estimate the magnitude of the change in $d\delta^*/dx$ due to TVC, and from this the change in pressure To fix ideas, consider the defining expression for the boundary-layer displacement thickness δ^*:

$$\int_0^{\delta^*} \rho_\delta u_\delta 2\pi r\, dy = \int_0^\delta (\rho_\delta u_\delta - \rho u) 2\pi r\, dy \quad \text{(A12)}$$

Here $r = r_w + y(\cos\alpha)$ is now variable in the thick boundary layer One sees that for $r \neq r_w$ the expression for δ^* is fundamentally different from the thin boundary-layer case ($r = r_w$ is assumed in the Mangler transformation) Yasuhara[16] gives the following results for the solution for δ^* in hypersonic flow:

With TVC

$$(\delta^*/r_w)_{\text{TVC}} \approx (1 + A m_e)^{1/2} - 1 \quad \text{(A13)}$$

Without TVC

$$(\delta^*/r_w)_M = (1/2) A m_{e_M} \quad \text{(A14)}$$

where, for a slender cone in hypersonic flow,

$$A = [1 + (\gamma - 1)M_\delta^2/2][(8C\mu_\delta)/(3\rho_\delta u_\delta \alpha^2 x)]^{1/2} \approx (\gamma - 1)(\tfrac{2}{3})^{1/2} \bar{\chi}_\delta / M_\delta \alpha \quad \text{(A15)}$$

One may approximate with sufficient accuracy for the present purpose Yasuhara's graphical results for m_e and m_{e_M} by

$$m_e \approx 1\,95 + (0\,36)A \qquad m_{e_M} = 1\,95 \quad \text{(A16)}$$

and replace M_δ by M_e and $\bar{\chi}_\delta$ by $\bar{\chi}$ defined by

$$\bar{\chi}_e \equiv M_e^3[(C\mu)/(\rho_e u x)]^{1/2} \quad \text{(A17)}$$

Now, define the change in the displacement thickness slope as follows:

$$\Delta(d\delta^*/dx)_{\text{TVC}} \equiv [(d\delta^*/dx)_{\text{TVC}} - (d\delta^*/dx)_{\text{VI}}] \quad \text{(A18)}$$

in which the last term is that computed from the viscous interaction (VI) solution With $r_w \approx \alpha x$, it may be shown from the preceding formulas that

$$\Delta(d\delta^*/dx)_{\text{TVC}} = \alpha[(-0\,49A - 0\,18A)/(1 + 1\,95A + 0\,36A^2)^{1/2} + (1 + 1\,95A + 0\,36A^2)^{1/2} - 1 - 0\,49A] \quad \text{(A19)}$$

The induced pressure correction may then be estimated by perturbing the VI solution as follows:

$$\Delta P_{\text{TVC}} \approx [\partial P/\partial(d\delta^*/dx)]\Delta(d\delta^*/dx)_{\text{TVC}} \quad \text{(A20)}$$

This may be put into the form

$$[(P/P_e) - 1]_{\text{TVC}} = [(P/P) - 1]_{\text{VI}} + (P_\infty/P)[\partial(P/P_\infty)/\partial\beta]_{\beta=\beta_{\text{VI}}} \times [1 + (d\delta^*/dx)^2_{\text{VI}}]^{-1} \times \Delta(d\delta^*/dx)_{\text{TVC}} \quad \text{(A21)}$$

The second term on the right is the local TVC pressure correction

For the TVC correction to the local skin friction, Yasuhara finds that approximately

$$C_{f_{\text{TVC}}} \approx \{1 + 0\,377A - 0\,0089A^2\} \quad \text{(A22)}$$

with zero pressure gradient, $Pr = 0\,7$, and $T_w/T = 1\,0$ The TVC effect is contained in the terms multiplied by A in the forementioned, so that

$$(C_{f_{\text{TVC}}} - C_{f_M})/C_{f_M} \approx \{0\,377A - 0\,0089A^2\} \quad \text{(A23)}$$

where the no-interaction skin-friction coefficient is

$$C_{f_M} = (\tfrac{1}{2}) K_w f_w''[(3\mu\, C)/(\rho\, u_e\, x)]^{1/2} \quad \text{(A24)}$$

For the TVC correction to total drag, then, one need only compute the change in pressure and skin-friction drag coefficients With $L = l\cos\alpha$, these are given by

$$(\Delta C_{D_p})_{TVC} = \left(\frac{4P_e}{\gamma P_\infty M_\infty^2 L^2}\right) \int_0^L \Delta\left(\frac{P}{P_e} - 1\right)_{\text{TVC}} Z dZ \quad \text{(A25)}$$

$$(\Delta C_{D_f})_{\text{TVC}} = \left(\frac{2}{L^2 \tan\alpha}\right)\left(\frac{P_e M^2}{P_\infty M_\infty^2}\right) \int_0^L C_{f_M} \times \{0\,377A - 0\,0089A^2\} Z dZ \quad \text{(A26)}$$

where the term under the integral in (A25) is the TVC correction term of Eq (A21)

Injection Drag

The passage of injected gas from the model walls into the boundary layer produces a drag force increment that is small, but not negligible If we assume the validity of the no-slip boundary condition,** then the injection velocity must be normal to the cone surface Let $\dot{m} = \rho_w v_w$ be the local mass flux Then the injection drag component may be computed from the flux of momentum across the porous surface as follows:

$$D_{\text{inj}} = \int_{A_1} (\dot{m}^2/\rho_w) \sin\alpha dA \quad \text{(A27)}$$

Since the magnitude of the injection drag turns out to be at most 10% of the total drag, a simple but fairly crude calculation is adequate It is assumed that $\dot{m} \approx M/A_{\text{slant}}$ (uniform injection) and ρ_w is taken to be roughly constant over the whole cone surface Employing the perfect gas law, then, one obtains

$$C_{D_{\text{inj}}} = [2\cos^4\alpha M^2 R_w T_w]/[\pi^2 L^4 \sin^2\alpha \rho_\infty u_\infty^2 P_w] \quad \text{(A28)}$$

Here P_w, T_w, and R_w are suitable average values for the surface pressure, temperature, and specific gas constant One should notice that $C_{D_{\text{inj}}}$ is roughly proportional to $\dot{M}^2$, and

** The effect of slip is to alter the injection angle However, a simple calculation shows that this effect can be neglected

hence becomes relatively important only at the higher injection rates In the present experiment, data are available to determine P_w and T_w The gas constant R_w is a function of mixture concentration and must be estimated for the helium injection case This estimate was based on Baron's results

References

[1] Talbot, L , Koga, T , and Sherman, P M , "Hypersonic viscous flow over slender cones," J Aeronaut Sci **26**, 723–730 (1959)

[2] Talbot, L , "Viscosity corrections to cone probes in rarefied supersonic flow at a nominal Mach number of 4," NACA TN 3219 (1954)

[3] Hayes, W D and Probstein, R F , *Hypersonic Flow Theory* (Academic Press, New York, 1959), Chap IX

[4] Maslach, G J and Talbot, L , "Low density aerodynamic characteristics for a cone at angle of attack," Univ of California Engineering Project Rept HE-150-172 (1959)

[5] Baron, J R , "The binary boundary layer associated with mass transfer cooling at high speeds," Massachusetts Institute of Technology, Naval Supersonic Lab , TR 160 (1956)

[6] Low, G M , "The compressible boundary layer with fluid injection," NACA TN 3404 (1955)

[7] King, H H , "Hypersonic flow over a slender cone with gas injection," Ph D Thesis, Univ of California Engineering Project Rept HE-150-205 (1962)

[8] Lynes, L L , "Design, fabrication, and evaluation of axisymmetric nozzles," Univ of California Engineering Project Rept HE-150-174 (1959)

[9] Maslach, G J and Sherman, F S , Design and testing of an axisymmetric hypersonic nozzle for a low density wind tunnel," Wright Air Development Div TR 56-341 (1956)

[10] Maslach, G J , "A precision differential manometer," Rev Sci Instr **23**, 367–369 (1952)

[11] Maslach, G J , "Vacuum facilities for the study of supersonic flow," Chem Eng Progr **48**, 594–598 (1952)

[12] Kopal, Z , Tables of supersonic flow around cones," Massachusetts Institute of Technology (1947)

[13] Sims, J L , "Supersonic flow around right circular cones, tables for zero angle of attack," Army Ballistic Missile Agency DA-TR-11-60 (1960)

[14] Gross, J F , Hartnett, J P , Masson, D J , and Gazley, C , Jr , "A review of binary boundary layer characteristics," Rand Corp Rept RM-2516 (1959)

[15] Probstein, R F and Elliott, R F , "The transverse curvature effect in compressible axially symmetric laminar boundary-layer flow," J Aeronaut Sci **23**, 208–225 (1956)

[16] Yasuhara, M , "Axisymmetric viscous flow past very slender bodies of revolution," J Aerospace Sci **29**, 667–680 (1962)

[17] Baron, J R and Scott, P B , "The laminar diffusion boundary layer with external flow field pressure gradients," Massachusetts Institute of Technology, Naval Supersonic Lab , TR 419 (1959)

[18] Freedman, S I , Radbill, J R , and Kay, J , "Theoretical investigations of a supersonic laminar boundary layer with foreign-gas injection," AIAA J **1**, 148–158 (1963)

[19] Bromley, L A and Wilke, C R , "Viscosity behavior of gases," Ind Eng Chem **43**, 1641–1648 (1951)

[20] Clutter, D W and Smith, A M O , "Solution of the general boundary layer equations for compressible flow, including transverse curvature," Douglas Aircraft Co Rept LB 31088 (1963); also Smith, A M O and Clutter, D W , 'Solution of the incompressible laminar boundary layer equations," AIAA J **1**, 2062–2071 (1963)